X-ray Three Beam Cases and the Influence of Lattice Defects

W. Scherz and G. Hildebrandt
Fritz-Haber-Institut der Max-Planck-Gesellschaft, Berlin-Dahlem

Z. Naturforsch. **36a**, 921–928 (1981); received July 10, 1981

The three beam cases {111, $\bar{1}11$; 200} (Case I) and {111, $\bar{1}\bar{1}1$; 220} (Case II) in germanium were examined with CuKα_1 radiation from a bent quartz monochromator crystal. For the intensity relation $I_0/(I_L+I_M)$, excellent agreement with previous measurements (Uebach) resulted for Case I; small deviations from a calculated value could be explained by theoretical arguments, considering the crystal as slightly imperfect. In Case II, which reacted more sensitively upon lattice defects, these deviations were much larger and in an unexpected direction. A first attempt of a "Three Beam Lang Topography" is reported.

1. Introduction

Monochromatic x-ray waves entering perfect crystals in directions which satisfy the Laue-Bragg-condition on one set of net planes create wave fields inside the crystal. Each one of these fields is a combination of two plane waves with wave vectors $\boldsymbol{K}_0$ and $\boldsymbol{K}_H$; the maximum amplitudes of the fields are arranged on planes parallel to the net planes with the same periodicity, and those fields which have their planes with maximum amplitudes far from planes of atoms undergo reduced absorption: Borrmann effect [1] (1941, 1950).

In this simplest case, which is usually considered, two points 0 and H of the reciprocal lattice lie on the Ewald sphere: two beam case. Theoretically and experimentally much more difficult to handle are three beam cases, when two kinds of net planes are set to interfere simultaneously, so that the Ewald sphere cuts three points (later on called 0, L, M). Now wave fields combined of three plane waves $\boldsymbol{K}_0$, $\boldsymbol{K}_L$, $\boldsymbol{K}_M$ are created, the maximum amplitudes of which are no longer arranged on planes, as in the two beam case, but on lines. However, reduced absorption has again to be expected if these lines are far from atoms: "enhanced" Borrmann effect, first detected by Borrmann and Hartwig [2] (1965), when the planes ($\bar{1}1\bar{1}$) and ($\bar{1}11$) in germanium were set to reflect CuKα radiation from a point source. Those waves $\boldsymbol{K}_0$, $\boldsymbol{K}_L$, $\boldsymbol{K}_M$ which underwent strongly reduced absorption produced three reflections R_0, R_L, R_M, which were observable on the film as three points with enhanced intensities superimposed at the intersection of the transmission lines $\bar{1}11$, $\bar{1}1\bar{1}$ and at appropriate places of the reflection lines $1\bar{1}\bar{1}$ and $1\bar{1}1$, which result from the usual Borrmann effect of the two beam case on {111}; in other words: the intensities of the reflections R_0, R_L, R_M of this three beam case were much higher than those of R_0, R_H of the related two beam case on {111}. Many details of this particular three beam case have been discussed theoretically (cf. [3]); calculated absorption coefficients and intensity distributions were in reasonable agreement with experiments [4].

Other three beam cases are usually much more difficult to handle, even the seemingly similar one with reflections on ($\bar{1}11$) and ($1\bar{1}1$). However this case is rather different from the first one, as can be shown by comparison with the well known Renninger "Umweganregungs-Effekt" [5], where the "Umweg" results from the difference of two wave vectors. In our cases the difference vectors are $\boldsymbol{K}_{\bar{1}1\bar{1}} - \boldsymbol{K}_{\bar{1}11} = \boldsymbol{K}_{00\bar{2}}$ and $\boldsymbol{K}_{\bar{1}11} - \boldsymbol{K}_{1\bar{1}1} = \boldsymbol{K}_{\bar{2}20}$, resp. In the diamond lattice, however, {200} is related to a "forbidden" reflection, but {220} to the strongest reflection. This suggests strong differences between our two cases, which should therefore be characterized as follows:

Case I: ($\bar{1}1\bar{1}$, $\bar{1}11/00\bar{2}$),
Case II: ($\bar{1}11$, $1\bar{1}1/\bar{2}20$).

A pseudo Kossel line diagram (CuKα, projection on (110) of Ge), restricted to the lines involved in these cases, is shown in Figure 1. The Borrmann-Hartwig experiment exhibited the points 1 (intersection between $\bar{1}11$ and $\bar{1}1\bar{1}$) and 2, 3 (intersections between lines {111} and {200}) with enhanced intensities. The other points 4, 5, 6 belong to Case II: 4 is the intersection between $\bar{1}11$ and $1\bar{1}1$, and 5, 6 are re-

Reprint requests to Prof. G. Hildebrandt, Fritz-Haber-Institut der Max-Planck-Gesellschaft, Faradayweg 4–6, D-1000 Berlin 33.

0340-4811 / 81 / 0900-0921 $ 01.00/0. — Please order a reprint rather than making your own copy.

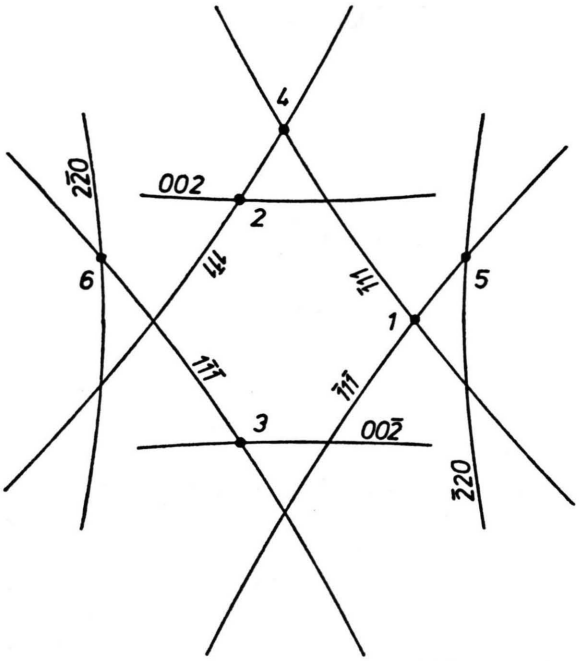

Fig. 1. CuKα Kossel line diagram of a (110) germanium plate. Only the lines involved in Case I (leading to points with enhanced intensities 1, 2, 3) and Case II (leading to 4, 5, 6) are drawn.

lated to {111} and {220}. Anyone of the waves $\boldsymbol{K}_1$, $\boldsymbol{K}_2$, $\boldsymbol{K}_3$ could excite the Case I (cf. [1]); the same holds for $\boldsymbol{K}_4$, $\boldsymbol{K}_5$, $\boldsymbol{K}_6$ in Case II. We restrict our considerations, however, to the symmetrical cases, were the incident waves are parallel to $\boldsymbol{K}_1$ (or $\boldsymbol{K}_4$, resp.).

The dispersion surface of Case I is easily calculable, and if the problem is simplified to the intersection with the plane of symmetry (001), even an analytical solution can be derived, as was shown earlier [3]. The fundamental equations for Case II are more difficult to handle (cf. the following chapter), but again the simplified problem can be solved analytically. This has been shown, together with some details of the theory (and more references on many beam cases), in [6].

Borrmann and Hartwig tried to demonstrate the enhanced effect also in Case II but they failed: Whereas in Case I clearly three points 1, 2, 3 (Fig. 1) with enhanced intensities (and the intensity relation $I_0 : I_L : I_M = 2 : 1 : 1$) were superimposed on the {111} lines, no enhanced transmitted wave $\boldsymbol{K}_0 = \boldsymbol{K}_4$ could be detected with the wide angle technique in the intersection of $\bar{1}11$ and $1\bar{1}1$, and points due to reflected waves $\boldsymbol{K}_L = \boldsymbol{K}_5$ and $\boldsymbol{K}_M = \boldsymbol{K}_6$ (5 and 6 in Fig. 1) — if present — would have been annihilated by the strong underlying {220} lines. Only by restricting the incident beam to the surrounding of $\boldsymbol{K}_0 = \boldsymbol{K}_4$ was it later on possible to make the points 5 and 6 visible [7], because the diagram then existed only of short parts of the weak {111} lines; but it still remained an open question whether $\boldsymbol{K}_4$ was supplied with enhanced intensity.

Uebach [4] improved the experimental arrangement by using a curved monochromator crystal in front of the specimen crystal. The adjustment — already difficult in many beam cases — became then even more complicated, but diagrams resulted with a decreased background opening the chance for more accurate intensity measurements and for the possibility to detect even weak reflections. By applying this technique, Scherz succeeded in observing the $\boldsymbol{K}_0$ reflection of Case II [8]; further new results are reported below.

2. Calculations

The calculation of the dispersion surface starts from the fundamental equations of the dynamical theory which can be written as follows [9]:

$$(2\,\varepsilon_m - \chi_0)\,\boldsymbol{D}_0 = \sum_{n \neq m} \chi_{m-n}\,\boldsymbol{D}_{N[m]} \qquad (1)$$

(n, m index triples; χ_{m-n} Fourier component of the dielectric susceptibility; $\boldsymbol{D}_{n[m]}$ component of the amplitude of the dielectric displacement $\boldsymbol{D}_n$ perpendicular to the wave vector $\boldsymbol{K}_m$;

$$\varepsilon_j = \tfrac{1}{2}(\boldsymbol{K}_j^2 - k^2)/\boldsymbol{K}_j^2$$

excitation errors). In three beam cases (1) takes the form

$$(2\,\varepsilon_0 - \chi_0)\,\boldsymbol{D}_0 = \chi_{\bar{L}}\,\boldsymbol{D}_{L[0]} + \chi_{\bar{M}}\,\boldsymbol{D}_{M[0]}, \qquad (2a)$$

$$(2\,\varepsilon_L - \chi_0)\,\boldsymbol{D}_L = \chi_L\,\boldsymbol{D}_{0[L]} + \chi_{L-M}\,\boldsymbol{D}_{M[L]}, \qquad (2b)$$

$$(2\,\varepsilon_M - \chi_0)\,\boldsymbol{D}_M = \chi_M\,\boldsymbol{D}_{0[M]} + \chi_{M-L}\,\boldsymbol{D}_{L[M]}. \qquad (2c)$$

Case I: $L - M = \bar{1}1\bar{1} - \bar{1}11 = 00\bar{2}$ belongs to a "forbidden" reflection, therefore $\chi_{L-M} = \chi_{M-L} = 0$: the right hand sides of (2b), (2c) are restricted to one term each, the calculation is simplified [3].

Case II: $L - M = \bar{1}11 - 1\bar{1}1 = \bar{2}20$, χ_{L-M} and χ_{M-L} are large, two term sums in all three equations make the calculation more difficult. However, as mentioned above, analytical solutions are possible in both cases if the calculation is restricted to the intersection of the dispersion surface with the resp.

plane of symmetry. The results can then be symbolized by

$$Q_{1,6} \cdot L_{3,4} \cdot Q_{2,5} = 0 \quad \text{(Case I)},$$
$$K_{1,2,3} \cdot Q_{4,5} \cdot L = 0 \quad \text{(Case II)},$$

where K are cubic, Q quadratic, L linear equations. The calculated dispersion lines are shown in Figures 2a, b.

As pointed out earlier by Ewald [10], [11] minimum absorption is related to those modes which have dispersion branches close to the Laue point La. Only wave fields belonging to these branches are able to penetrate thick crystals. From this argument it is concluded (and justified by calculation) that minimum absorption belongs to Q_1 in Case I and maximum absorption to Q_6. The resp. branches in Case II are K_1 and K_3 (in both cases the linear solutions are not excited within the plane of symmetry).

Along one branch the absorption is not constant: it changes the more, the stronger the curvature of the branch. We try to make this point clear by a comparison with the two beam case. If δ denotes the angle between a particular Poynting vector $\boldsymbol{S}$ (giving the energy flow direction of a wave field) and the Poynting vector of the wave field with minimum absorption (polarized vertical to the plane of incidence), the absorption in direction of $\boldsymbol{S}$ is given by (Eq. (34.39) in [9])

$$\mu_S = \frac{\mu_0}{\cos\theta_B}\left\{\cos\delta - \frac{A}{\sin\theta_B}\sqrt{\sin^2\theta_B - \sin^2\delta}\right\} \quad (3)$$

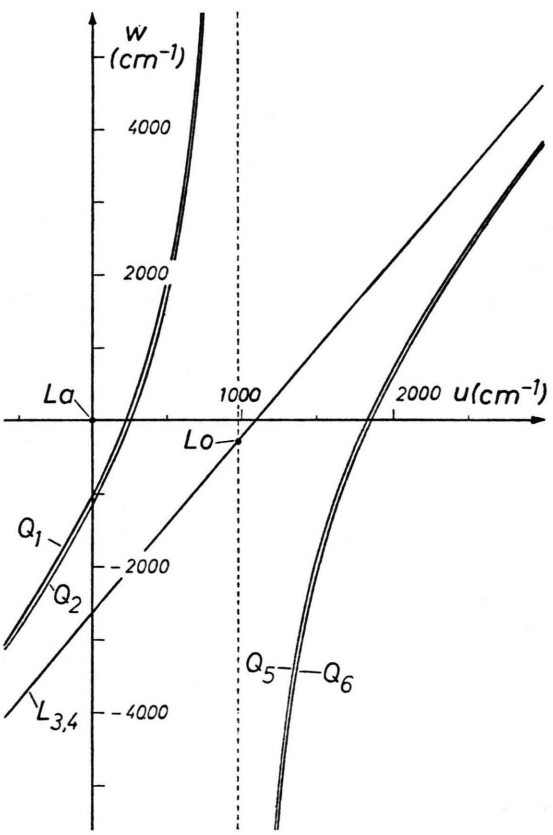

2a)

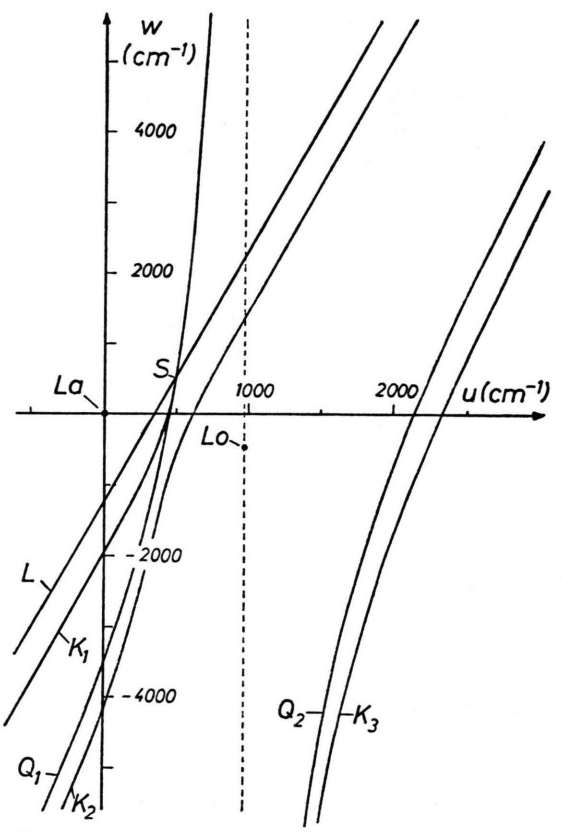

2b)

Fig. 2. Dispersion surface. — La Laue point; Lo Lorentz point; u axis in direction of incidence, $\boldsymbol{s}_0$; different scales on u and w. 2a: Case I, intersection with symmetry plane (001); Q_1, Q_6 and Q_2, Q_5 are quadratic, $L_{3,4}$ are linear solutions of the fundamental equations; the smallest absorption is related to Q_1. 2b: Case II, intersection with $(1\bar{1}0)$; $K_{1,2,3}$ cubic, $Q_{1,2}$ quadratic, L linear solutions; small absorption related to K_1 and Q_1; near La, the curvature of K_1 is stronger than that of Q_1 in Case I.

(μ_0 linear absorption coefficient, θ_B Bragg angle, $A = |\chi_{iH}^{\perp}/\chi_{i0}|$, where χ_i are imaginary parts of χ); μ_S changes with δ as

$$\frac{d\mu_S}{d\delta} = \frac{\mu_0}{\cos\theta_B}\sin\delta \cdot \left\{\frac{A}{\sin\theta_B}\frac{\cos\delta}{\sqrt{\sin^2\theta_B - \sin^2\delta}} - 1\right\}. \quad (4)$$

In Fig. 3, μ_S and $d\mu_S/d\delta$ (calculated with $\theta_B = 20°$, $|\chi_{iH}/\chi_{i0}| = 0.95$, $\mu_0/\cos\theta_B = 300\ cm^{-1}$) are shown as a function of δ. There is a strong increase of μ_S, and even of $d\mu_S/d\delta$, with increasing δ; but since the Poynting vector is always directed perpendicular to the resp. branch, a strong increase of δ (and thus of the absorption) is caused by a strong curvature of the branch. Therefore Case II (with stronger curvature of the branch with minimum absorption) should be expected to react more sensitively to lattice defects than Case I.

In experiments the intensity relations between $|D_0|^2$, $|D_L|^2$ and $|D_M|^2$ can be measured with a relatively high degree of accuracy. In our symmetrical three beam cases $|D_L|^2 = |D_M|^2$ holds not only for incident waves entering the crystal in directions parallel to the plane of symmetry, but also, due to symmetry arguments, for the integrated intensities. The Poynting vector

$$\boldsymbol{S} \propto \boldsymbol{s}_0 |D_0|^2 + \boldsymbol{s}_L |D_L|^2 + \boldsymbol{s}_M |D_M|^2 \quad (5a)$$

treated in the simplified form

$$\boldsymbol{S}_s \propto \boldsymbol{s}_0 |D_0|^2 + (\boldsymbol{s}_L + \boldsymbol{s}_M) |D_{L,M}|^2 \quad (5b)$$

($\boldsymbol{s}_j$ are unit vectors parallel to $\boldsymbol{K}_j$) is then representative for some properties of our two cases. Since $\boldsymbol{S}_s$ is perpendicular to the branch, $|D_0|^2/|D_{L,M}|^2$ can easily be calculated from the mentioned analytical solutions, and conclusions can be drawn in connection with experiments.

Let β denote an angle between the incident wave fulfilling the Laue-Bragg condition exactly ($\beta = 0$) and an actual direction of incidence (within the plane of symmetry; the + sign means a deviation in direction towards $\boldsymbol{s}_0$;) then from the branch with minimum absorption the following figures for α (angle between $\boldsymbol{S}_s$ and $\boldsymbol{s}_0$) and $R(|D_0|^2/|D_{L,M}|^2$, relative value; $R = 1$ if $\beta = 0$) have been calculated, cf. Table 1:

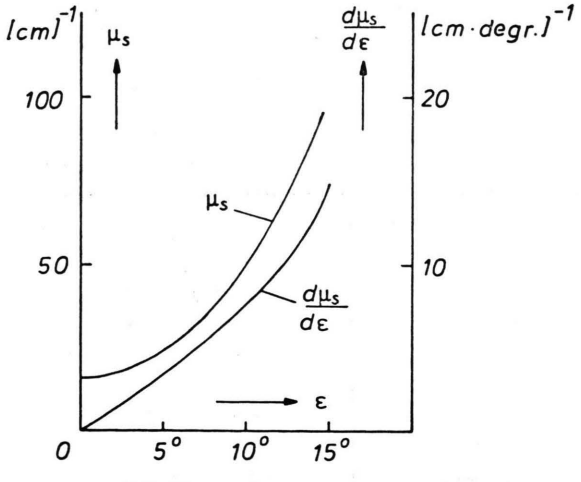

Fig. 3. μ and $d\mu/d\varepsilon$ as a function of ε; cf. text.

The following conclusions can be drawn from Table 1:

a) From $\beta = -3.2''$ to $\beta = +3.2''$, $R = |D_0|^2/|D_{L,M}|^2$ changes by a factor 2.6 in Case I, but 18.2 in Case II: again Case II should react more sensitive against lattice deformations.

b) In both cases R is much more changed by a deviation $+\beta$ than by a deviation of the same amount in the opposite direction, $-\beta$. Assuming statistically distributed defects we have thus to expect that measured values R_{exp} of real crystals be always a little larger than the values R_{th} calculated for perfect crystals. This might explain the fact that in Uebachs measurements [4] (Case I) all values $I_L/I_0 = I_M/I_0$ were systematically lower than theoretically expected.

	Case I			Case II		
β	α	$\lvert D_0\rvert^2 : \lvert D_{L,M}\rvert^2$	R	α	$\lvert D_0\rvert^2 : \lvert D_{L,M}\rvert^2$	R
$+3.2''$	8.4°	3.22 : 1	1.61	4.5°	4.54 : 1	2.79
0	11.0°	2.00 : 1	1.00	8.3°	1.63 : 1	1.00
$-3.2''$	13.6°	1.24 : 1	0.62	13.8°	0.25 : 1	0.15

Table 1. Calculated intensity relations in both cases for two deviations ($\beta = \pm 3.2''$) of the incident radiation from the exact Bragg direction. Ge, CuKα.

3. Experiment

The experimental arrangement is shown in Figure 4. CuKα_1 radiation from a fine focus tube RR (line focus F perpendicular to the plane of the figure) was focused by a bent quartz monochromator crystal M onto the axis of a diffractometer G. The specimen crystal K was adjusted to Case I or II in such a way that, while the reflection R_0 (in direction of the incident beam) remained in the plane of Fig. 4, R_L and R_M were diffracted in symmetrical directions below and above this plane (then R_h in Fig. 4 would be the projection of both reflections; actually Fig. 4 is drawn for reflection in a two beam case). A scintillation counter Z or a photographic plate P were used to record the reflections.

As specimen crystals germanium plates with surfaces parallel (deviation less than 10′) to (110), etched with CP 4, were used. One plate with thickness $t = 0.98$ mm contained dislocations, two others with $t = 0.37$ and $t = 1.097$ mm were dislocation-free.

As already mentioned, the crystals were adjusted only for the symmetrical three beam cases (incident waves directed to point 1 in Case I or point 4 in Case II, resp., cf. Figure 1). This alignment cannot be done directly with thicker crystals due to the very weak intensities of the {111} reflections. But since the points 1 (or 4) are on common lines with two {220} intersections of high intensity (not shown in Fig. 1), the latter have been used as an aid for finding the {111} intersections.

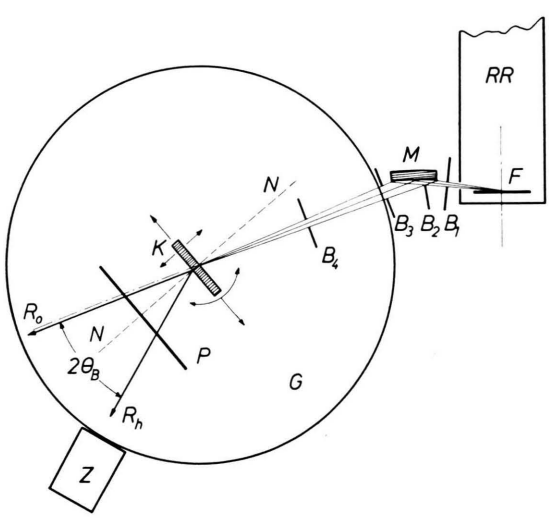

Fig. 4. Experimental arrangement. RR x-ray tube with fine line focus F ($\perp$ to plane of figure); M bent quartz monochromator, set for CuKα_1; G diffractometer with specimen crystal K; R_0, R_h reflections drawn for a two beam case; Z scintillation counter; P photographic plate; B slits.

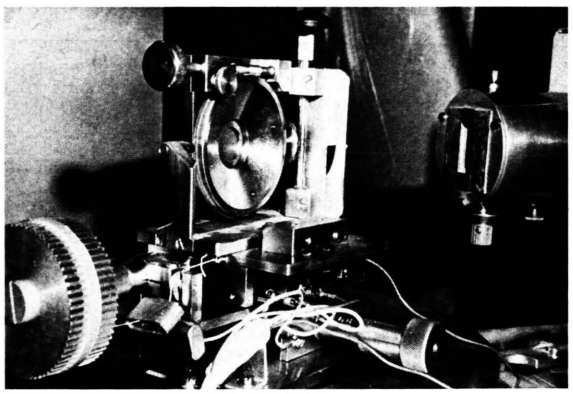

Fig. 5. Photo of crystal holder mounted on a table which allows for a travers motion. Right: entrance slit of the counter.

Later on the crystal holder together with the photographic plate was placed on a glide table which allowed for a precise lateral displacement with the help of a motor. With this arrangement three beam topographs have been taken similar to the Lang topographs [12] in the two beam case. Figure 5 presents a photo of the experimental arrangement.

4. Results

4.1. As an example Fig. 6 demonstrates the efficiency of this experimental arrangement *. The dislocation-free germanium plate with thickness 1.097 mm was adjusted to Case I ($\bar{1}11$, $\bar{1}1\bar{1}/002$) for CuKα_1 radiation. The lines R_0 (right) and R_L and R_M (left, weaker) seem to be undisturbed; there is no indication of troublesome background (the consideration of background was one of the main sources of error in Uebach's evaluations of his experiments [4]).

The diagram in Fig. 6 is overexposed. Similar exposures with densities in the linear range have been evaluated with a densitometer. The result for the intensities of the reflections R_0, R_L, R_M was $I_L = I_M$ (within the limits of experimental error) and $(I_L + I_M)/2\,I_0 = 0.435 \pm 4\%$. This can be compared with theory: Calculated values for the integrated

* In Figs. 6 to 9 the R_j-lines are in the same positions as the enhancement points in Figure 1.

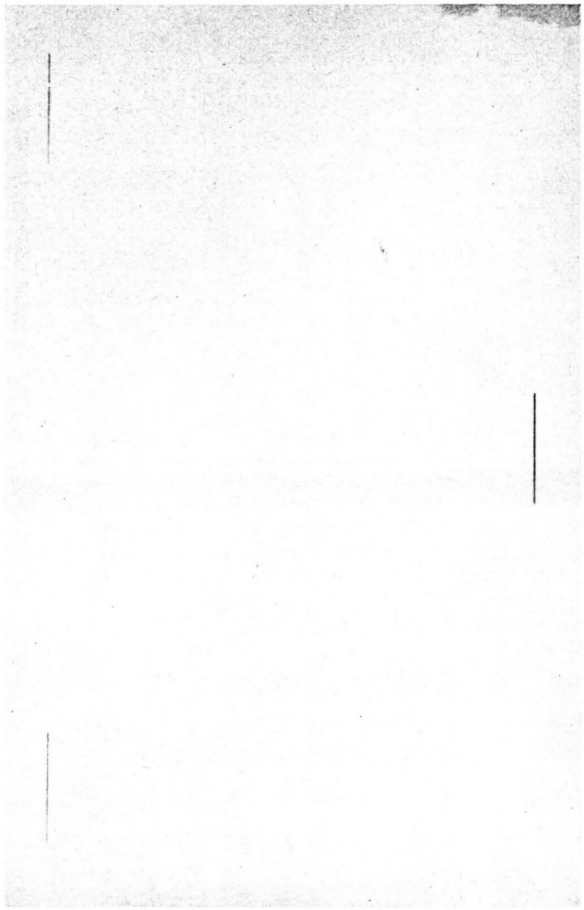

Fig. 6. Experimental diagram of Case I. (110) Ge plate, $t = 1.097$ mm; CuKα_1, 34 kV/24 mA/6 h. Right: R_0; left: R_L, R_M.

intensities at $t = 1.097$ mm have been contributed by Uebach [13] and Umeno [14] (unpublished). These values deviate by 2.6% from each other — possibly a result of different ranges for the integration. The experimental value is 1.4% below Uebach's and 4.0% below Umeno's calculated value, cf. Table 2.

Nevertheless this new experimental figure fits exactly to the values measured by Uebach [4] which, as mentioned in Chapt. 2, were altogether a little lower than the calculated ones. The new value thus states again a possible influence of small lattice defects, not visible in the diagram, leading to a too strong R_0 value, in accordance with the above theoretical expectation.

Table 2. Comparison between measured and calculated relations of integrated intensities (Case I).

	Theory		Experiment
	Umeno	Uebach	Scherz
$\frac{I_L + I_M}{2I_0}$	0.453	0.441	0.435 ± 0.017

4.2. In a second series of experiments the 1.097 mm thick crystal mentioned in 4.1 was adjusted for Case II, ($\bar{1}11$, $1\bar{1}1/\bar{2}20$). Whereas in Case I the diagram Fig. 6 with undisturbed lines had been obtained, the lines of Case II now exposed some irregularities. Only after a new short etching with CP 4 the diagram Fig. 7 with uniform lines could be obtained. Besides the R_L and R_M lines, the reflection R_0 became clearly visible, but at the expense of a very long overexposure (48 hours).

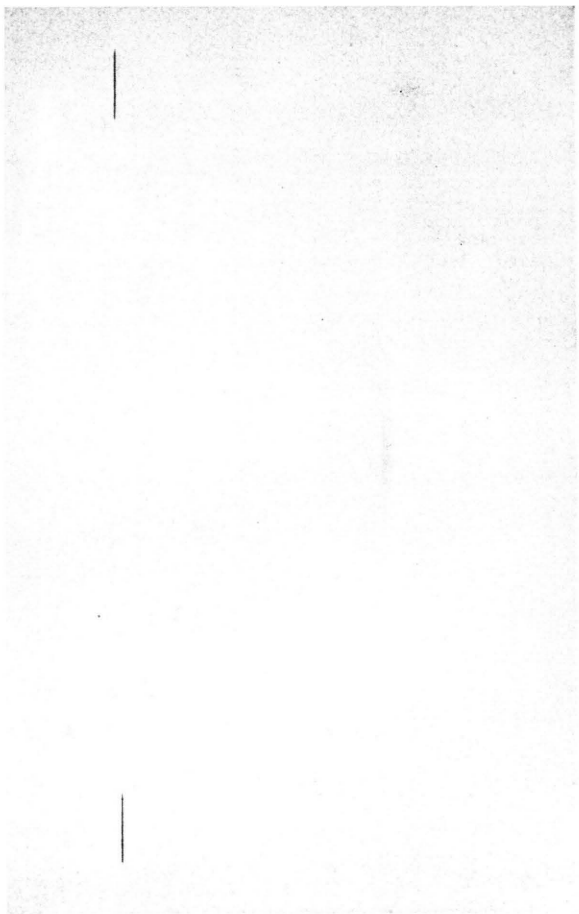

Fig. 7. Diagram of Case II; same conditions as in Fig. 6, but exposure time 48 h. Left: R_L, R_M; right: (very faint): R_0.

The measurement of an acceptably accurate value for $(I_L + I_M)/2\,I_0$ (Case II) was difficult under these circumstances because I_L and I_M had to be determined from a film with relatively short exposure time, I_0 however from a different, much overexposed film. For this reason the obtained experimental value

$$(I_L + I_M)/2\,I_0 = 11$$

was uncertain to at least 20%. The theoretically expected value, calculated by Umeno [14], was 8.0 and thus lower by 27% (from the mentioned theoretical considerations, however, we would rather have expected to get a too low experimental value).

Replacing the "perfect" Ge plate by a somewhat thinner crystal ($t = 0.98$ mm) with a dislocation density of about 1000 cm^{-2}, we obtained diagrams with strongly disturbed lines and a relative increase in the R_0 intensity. Using a nuclear plate (emulsion thickness 25 μm) an exposure time of 150 hours was necessary to get the diagram Figure 8a. A defect structure is there to be seen not only in R_L and R_M, but also in R_0 (enlarged in Fig. 8b); but it is hard to decide whether this structure is exactly the same in all reflections.

In order to answer this question we made an attempt to obtain a "three beam topograph" of our crystal. For this purpose the arrangement shown in Fig. 5 was added which allowed a precise lateral movement of the crystal together with the photographic plate. A topograph achieved with this arrangement is shown in Figure 9. It reveals clearly a somewhat different structure in R_L and R_M. So this kind of topography yields more information than the usual method using the two beam case — at least in principle, but at the expense of a more difficult adjustment, a complicated theoretical background and a long exposure time (which, however, could be shortened drastically by using synchrotron radiation).

A first attempt to evaluate the comparison of two beam and three beam intensities for the detection of lattice defects in a particular case has been reported elsewhere [15].

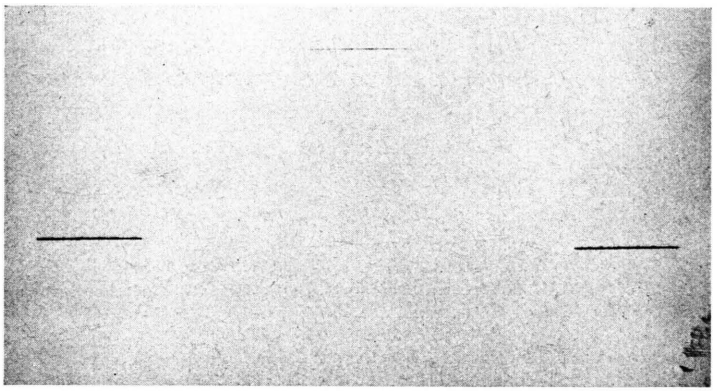

8a)

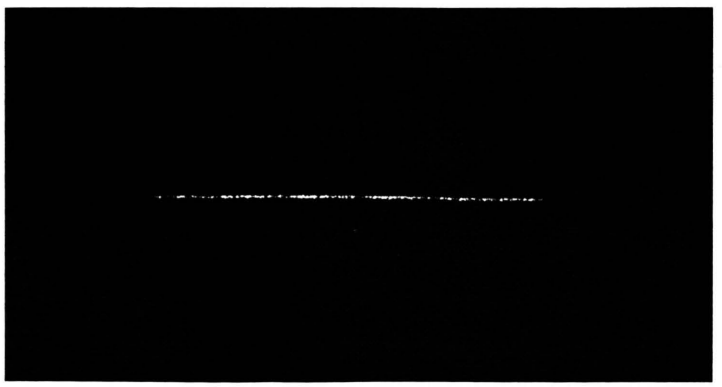

8b)

Fig. 8. Case II; 0.98 mm thick Ge plate with about 1000 dislocations/cm^2. Nuclear emulsion plate, 34 kV /24 mA/150 h. 8a) Complete diagram. 8b) R_0 only, enlarged.

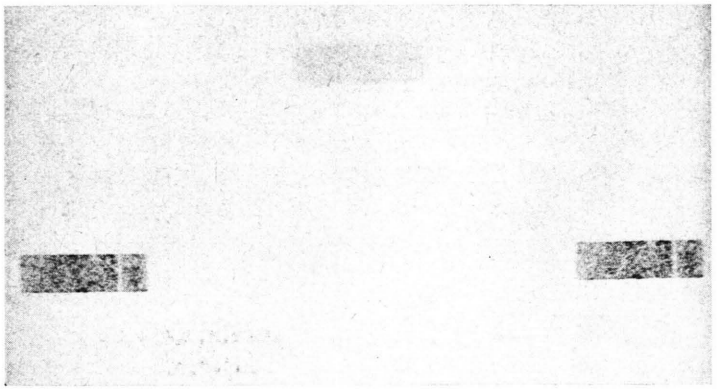

Fig. 9. "Three beam Lang topograph", taken in Case II of the 0.98 mm thick Ge plate. 34 kV/24 mA/10 h per 1 mm; 2.5 times enlarged. — The reflections R_L and R_M exhibit a somewhat different structure.

5. Conclusions

The experimental arrangement using a monochromator crystal has proved to be very suited for precise intensity measurements in three beam cases. In Case I small deviations between measured intensities and those predicted by the (perfect crystal) theory already observed by Uebach have been confirmed (although only in one point) with a higher precision, and the explanation (influence of small lattice defects) seems very likely from theoretical considerations. In Case II the intensity measurements resulted in values which deviated nearly by 1/3 from theory in an unexpected direction. So there remain open questions.

On the one hand, further measurements with perfect crystals in both cases seem to be necessary; the use of monochromatized, highly polarized synchroton radiation would considerably simplify the comparison of the intensities of Case I with those of Case II and of both with theory. Such measurements are in preparation.

On the other hand, measurements with less perfect crystals should go parallel with the attempt of establishing a simple theory of three beam cases in slightly deformed lattices, possibly comparably to the Penning-Polder theory [16] of the two beam case. Using synchroton radiation, three beam topography could be established with much shorter exposure times, due to the more favourable properties of the incident radiation.

[1] G. Borrmann, Physik. Z. **42**, 157 (1941); Z. Physik **127**, 297 (1950).
[2] G. Borrmann and W. Hartwig, Z. Kristallogr. **121**, 401 (1965).
[3] G. Hildebrandt, Phys. stat. sol. **24**, 245 (1967).
[4] W. Uebach, Z. Naturforsch. **28a**, 1214 (1973).
[5] M. Renninger, Z. Kristallogr. **97**, 107 (1937).
[6] G. Hildebrandt, Krist. Techn. **13**, 1095 (1978).
[7] G. Hildebrandt, Phys. stat. sol. (a) **15**, K83 (1973).
[8] G. Hildebrandt and W. Scherz, Acta Cryst. **A34**, S232 (1978).
[9] M. v. Laue, Röntgenstrahl-Interferenzen, Akadem. Verl. Ges. Frankfurt (Main) 1960.
[10] P. P. Ewald, Rev. Mod. Phys. **37**, 46 (1965).
[11] P. P. Ewald and Y. Héno, Acta Cryst. **A24**, 5 (1968); Y. Héno and P. P. Ewald, Acta Cryst. **A24**, 16 (1968).
[12] A. R. Lang, Acta Cryst. **12**, 249 (1959).
[13] W. Uebach, unpublished calculation.
[14] M. Umeno, unpublished calculation.
[15] M. Umeno and G. Hildebrandt, Z. Naturforsch. **35a** 342 (1980).
[16] P. Penning and D. Polder, Philips Res. Repts. **16**, 419 (1961).